Reconstruction of the Statistical Characteristics of Electric Fields in Enclosures With an Aperture Based on Random Forest Regression

Yuan Zhao, Xiang Zhao, Liping Yan, *Senior Member, IEEE*, Zhengyang Liu, Qiang Liu, Changjun Liu, *Senior Member, IEEE*, Haijing Zhou, and Kama Huang, *Senior Member, IEEE*

***Abstract*—In this paper, a random forest regression (RFR) is proposed to reconstruct the statistical characteristics of electric fields in perforated enclosures. The power balance method and a diffusion equation–based model have been applied to the analysis of such problems; however, they are unable to account for the statistical nonisotropy problem. To solve it, RFR is used to predict the variances of six basic electric fields, the real and imaginary parts of the three rectangular electric field components, in perforated enclosures under external excitation. Using the predicted variances, the probability density function to represent each basic electric field can be generated as they are assumed to obey normal distribution with zero mean value. Then the statistical characteristics of other electric fields can be calculated by an analytical method and Monte Carlo method. Using the proposed method relies on RFR, the overall statistical characteristics of electric fields in perforated enclosures with the electric dimensions less than ten times the wavelength can be accurately reconstructed. Using the predicted statistics, the practical electromagnetic compatibility problem, such as global shielding effectiveness of a perforated enclosure, can be evaluated in seconds.**

***Index Terms*—Aperture coupling, electric fields reconstruction, global shielding effectiveness, Monte Carlo method, perforated enclosure, random forest regression, statistical analysis.**

I. Introduction

THE study of electromagnetic (EM) properties in perforated enclosures under external excitation is an indispensable part of electromagnetic compatibility (EMC). Internal devices would respond to external electromagnetic interference (EMI) penetrated through apertures which have numerous dimensions for different purposes such as ventilation, signal exchange, and power supply that compromise the shielding effectiveness [1], [2]. In order to analyze these EMC problems, many numerical methods based on Maxwell's equations have been developed in the past [3]. However, in the cases of electrically large problems, two difficulties would commonly be encountered.

1) The well-known immense computational cost. Any changes in any parameters of the geometrical configuration require recalculation of the new model which is resource consuming.
2) The high frequency response sensitivity (HFRS). HFRS refers to the phenomenon that at relatively high excitation frequency, small changes in the boundary and/or excitation conditions can cause greater changes in the spatial distribution patterns of the electric fields [4].

HFRS is the intrinsic feature of electrically large problems, regardless of which analysis method is used. However, statistical methods have shown effectiveness in overcoming this problem [5], [6]. The well-known power balance (PWB) method has been proposed to analyze the high frequency EM coupling of complex cavities, such as consisting of different aperture and cavity structures with internal contents, based on conservation of energy and some statistical assumptions [7]–[13]. In principle, the PWB method is a back-of-the-envelope calculation, in which the EM field inside a perforated enclosure is considered to be similar to the reverberation chamber, and consequently be statistically uniform, isotropic, and randomly polarized. However, in many cases of the perforated enclosure, the statistical assumptions adopted in the PWB method may not be met well. A diffusion equation–based model has been proposed to describe nonuniform diffuse EM fields inside electrically large enclosures, and it is thought to be a natural generalization of the PWB method [14]–[16]. However, the statistical nonisotropy of the fields has still not been dealt with in the diffusion equation–based model. It is implied in [14] that the inhomogeneities in the field only arise when the absorption in the walls and contents of the enclosure is significant, but the nonisotropy is very apparent even in the case of low losses for the perforated enclosures. For example, as we can see next in this paper, the variances of the real and imaginary parts of the three orthogonal electric field components inside the enclosure are obviously different, and as a result, one orthogonal component is much weaker than the other two. In fact, it is the statistical characteristics of the component fields that ultimately determine the statistical characteristics of the total field.

Manuscript received January 18, 2019; revised May 18, 2019; accepted June 14, 2019. Date of publication September 27, 2019; date of current version August 13, 2020. This work was supported in part by National Science Foundation (NSF) under Grant 61877041 and in part by NSAF Grant U1530143 of China. *(Corresponding author: Xiang Zhao.)*

Y. Zhao, X. Zhao, L. Yan, Z. Liu, C. Liu, and K. Huang are with the College of Electronics and Information Engineering, Sichuan University, Chengdu 610065, China (e-mail: zhaoyuanscu@hotmail.com; zhaoxiang@scu.edu.cn; liping_yan@scu.edu.cn; sculiuzhengyang@163.com; cjliu@ieee.org; kmhuang@scu.edu.cn).

Q. Liu and H. Zhou are with the Institute of Applied Physics and Computational Mathematics, Beijing 100088, China (e-mail: q_liu1987@126.com; zhou-haijing@vip.sina.com).

Color versions of one or more of the figures in this paper are available online at http://ieeexplore.ieee.org.

Digital Object Identifier 10.1109/TEMC.2019.2926521

In our previous work [17], some graphic tools that provide a quick reference for the averages, variances, and probability density functions (PDFs) of component electric fields under different structural dimensions are shown and the nonisotropy of the electric fields is apparent. In addition, it can be found that the statistics of the electric fields in perforated enclosures are fairly insensitive to the perturbations of the boundary and/or excitation conditions. Inspired by the good regularity of the statistics, it is feasible and necessary to build relationships between the essential structural dimensions of a perforated enclosure and its internal electric field statistics.

In this paper, random forest regression (RFR) is adopted to predict the key statistics, which are the variances of the real and imaginary parts of the three rectangular electric field components in perforated enclosures. RFR is an ensemble machine learning method that operates by constructing a multitude of decision trees and its output is the average of the prediction for each decision tree. The training set for each decision tree is randomly sampled from the original training set with replacement. In this way, it generates an internal unbiased estimate of the generalization error and can overcome overfitting problem during the training procedure [18], [19]. The RFR performs as a transfer function that builds the relationships between the structural dimensions of the perforated enclosures and their key internal electric field statistics. With the predicted results from RFR, the complete statistical characteristics of electric fields can be reconstructed through the use of two methods. An analytical method which uses a formula to derive the closed-form expression of the statistics for a dependent variable from the PDF of the known independent variable [20], and Monte Carlo (MC) method [21]. After the reconstruction, properties of a perforated enclosure such as the global shielding effectiveness (GSE) [22] can be quickly obtained. The proposed method will eliminate the need to repeat the numerical simulation for the perforated enclosures under different computational conditions, such as the excitation frequencies of the incident plane wave and the dimensions of enclosures and apertures.

This paper is organized as follows. Section II gives a brief review of the statistical results of electric fields in perforated enclosures. Section III focuses on the establishing RFRs. Section IV uses an example perforated enclosure to present the process of reconstructing the statistical characteristics of its internal electric fields based on the predicted variances. The conclusion follows in Section V.

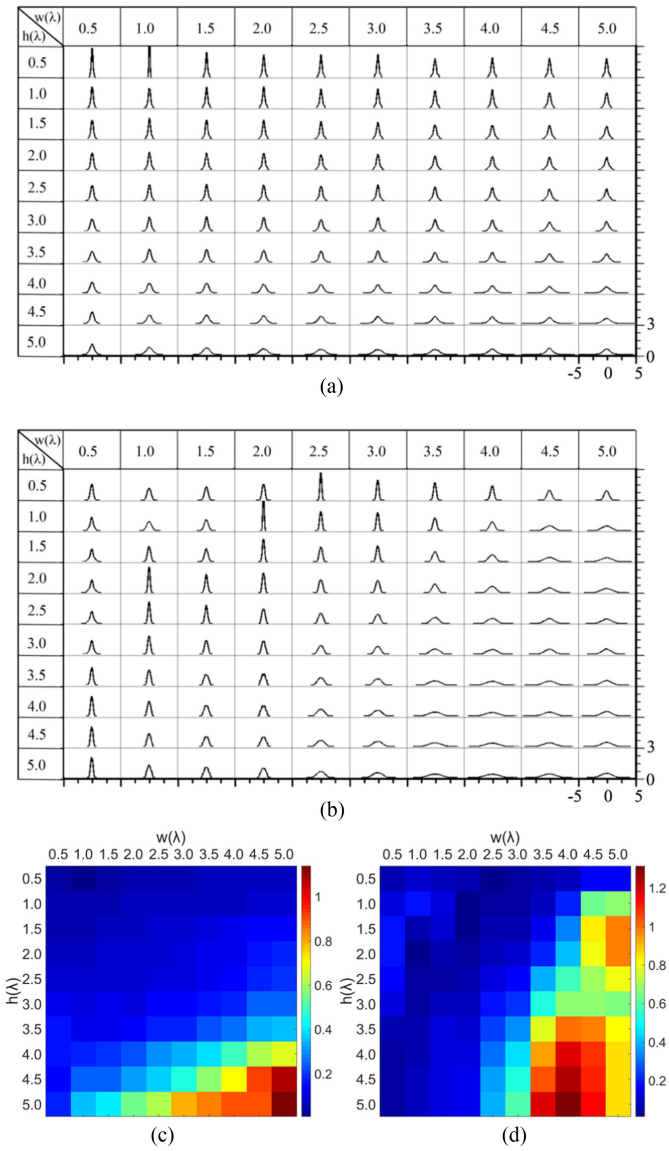

Fig. 1. PDFs and the variances of the real part of one complex rectangular electric field component in perforated enclosures (The first enclosure dimensions are $7.5\lambda \times 7.5\lambda \times 7.5\lambda$ and the second enclosure dimensions are $10.0\lambda \times 10.0\lambda \times 10.0\lambda$) versus different aperture sizes $w(\lambda)$ and $h(\lambda)$. (a) PDFs for first enclosure. (b) PDFs for second enclosure. (c) Color image of variances for first enclosure. (d) Color image of variances for second enclosure. Pictures (a) and (b) are extracted from [17].

II. Regularity of the Electric Field Statistics in Perforated Enclosures

In this section, a brief review of regular electric field statistics in perforated enclosures is given. The basic model studied in [17] is an enclosure with an aperture under external plane wave normal illumination. Two models are selected for illustration in this section. The dimensions of these two perforated enclosures are $7.5\lambda \times 7.5\lambda \times 7.5\lambda$ and $10.0\lambda \times 10.0\lambda \times 10.0\lambda$, where λ is the wavelength of the incident plane wave. These two perforated enclosures have been analyzed using a numerical method under different aperture dimensions to observe the statistical properties of their internal electric fields. The initial size of the aperture on both enclosures is $0.5\lambda \times 0.5\lambda$. It is then extended to the maximum size of $5.0\lambda \times 5.0\lambda$ with step length 0.5λ along two axis directions which correspond to the width and height of the aperture, respectively. Whatever the aperture size is, the aperture center remains located at the illuminated enclosure wall center. In [17], the PDFs of electric fields are calculated and some graphic lookup tables are formed, such as the PDFs and the variances of the real part of one complex rectangular electric field component shown in Fig. 1.

For convenient comparison, the axis values of the PDF curves are only shown at the bottom right corner in Fig. 1(a) and (b), and the other PDF curves have the same axis ranges. The horizontal

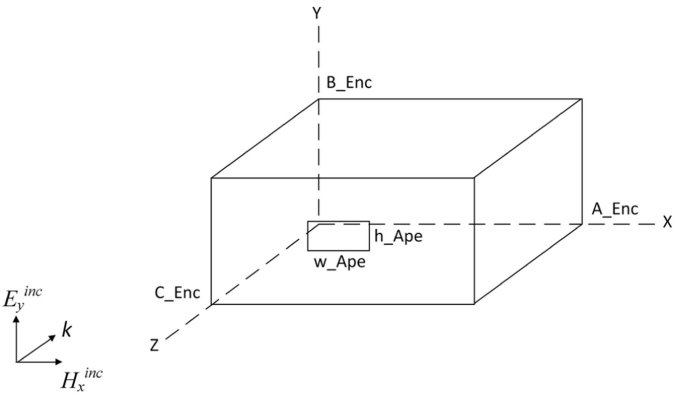

Fig. 2. Typical structure of an enclosure with a rectangular aperture.

axis represents the range of the field value. The vertical axis represents the range of the PDF value. It is obvious that the PDFs approximately obey normal distribution with zero mean value with different aperture dimensions, and they are changing gradually and "monotonically" from sharp (smaller variance) to flat (larger variance), as shown in Fig. 1(a) and the lower right part in Fig. 1(b) corresponding to the relatively large apertures. For the relatively small apertures in Fig. 1(b) the PDFs exhibit "nonmonotonous" trends, resulting from the complex coupling between enclosure and aperture. PDFs are simple and effective in describing the statistical properties of the electric fields in perforated enclosures. By combining with the specific variances, represented in the color images in Fig. 1(c) and (d), clearer changing trends based on aperture dimensions can be obtained.

Inspired by the stable and representative statistical results, reliable predictions of the electric field statistics in perforated enclosures can be achieved using RFR. The predicted targets are the variances of the real and imaginary parts of the three rectangular electric field components E_{xr}, E_{xi}, E_{yr}, E_{yi}, E_{zr}, and E_{zi}, which denoted as $\sigma^2_{E_{xr}}$, $\sigma^2_{E_{xi}}$, $\sigma^2_{E_{yr}}$, $\sigma^2_{E_{yi}}$, $\sigma^2_{E_{zr}}$, and $\sigma^2_{E_{zi}}$. The variances can be used to generate normal distributions which can approximately represent their PDFs. Then, based on statistical theory and the MC method, it is feasible to calculate the statistical properties of other electric fields.

III. Establish Random Forest Regression Models

The typical configuration of an enclosure with a rectangular aperture is shown in Fig. 2.

To train RFRs, five essential structural parameters of a perforated enclosure are selected as the input data. They are the electric dimensions of the enclosures and the rectangular apertures as given in (1)

$$X = [A\_Enc_i,\ B\_Enc_i, C\_Enc_i, w\_Ape_i, h\_Ape_i] \quad (1)$$

where $i = 1, 2, \ldots, N$, and N is the number of samples in training sets.

The perforated enclosures are illuminated by an external plane wave polarized in y direction with $|\vec{E}_y^{\,\mathrm{inc}}| = 1$ V/m, and propagating in $-z$ direction. The values of electric fields at each sampling point within the overall interior enclosure space are calculated by full wave simulation using j electromagnetic solver-finite difference time domain (JEMS-FDTD) [23]. The statistics of electric fields can then be obtained, such as $\sigma^2_{E_{xr}}$, $\sigma^2_{E_{xi}}$, $\sigma^2_{E_{yr}}$, $\sigma^2_{E_{yi}}$, $\sigma^2_{E_{zr}}$, and $\sigma^2_{E_{zi}}$ which are the predicted targets of RFRs. In order to improve the prediction accuracy, six independent RFRs are established to predict the six variances, respectively.

TABLE I
Perforated Enclosure Datasets for Training and Testing RFRs

Enclosures(λ)			Apertures(λ)		Step Length(λ)
A_Enc	B_Enc	C_Enc	w_Ape	h_Ape	
5.00	4.70	1.70	0.42-2.50	0.42-2.50	0.42
5.00	2.70	3.70	0.25-2.25	0.25-1.25	0.50
5.00	2.00	5.00	0.25-2.25	0.25-0.75	0.50
5.80	5.00	2.00	0.42-2.92	0.42-2.50	0.42
5.00	4.00	3.20	0.25-4.25	0.25-2.25	0.25
5.50	4.70	2.50	0.42-2.92	0.42-2.50	0.42
6.00	4.00	3.00	1.00-3.00	0.40-1.40	0.25
4.20	4.20	4.20	0.25-1.75	0.25-1.75	0.50
7.50	5.00	2.00	0.42-3.75	0.42-2.50	0.42
6.60	4.00	3.00	1.00-3.00	0.40-1.40	0.25
6.00	3.20	4.40	1.00-3.00	0.40-1.40	0.25
6.00	2.40	6.00	0.50-3.00	0.50-1.00	0.50
6.00	6.00	2.40	0.50-3.00	0.50-3.00	0.50
7.20	4.00	3.00	1.00-3.00	0.40-1.40	0.25
6.00	5.00	3.00	1.00-3.00	0.40-1.40	0.25
7.20	4.00	4.00	1.00-3.00	0.40-1.40	0.25
5.30	6.70	3.30	0.42-2.50	0.42-3.33	0.42
5.80	7.00	3.00	0.42-2.92	0.42-3.33	0.42
5.80	7.00	3.30	0.42-2.92	0.42-3.33	0.42
5.80	7.00	3.60	0.42-2.92	0.42-3.33	0.42
7.20	4.00	4.40	1.00-3.00	0.40-1.40	0.25
7.20	4.00	4.60	1.00-3.00	0.40-1.40	0.25
6.70	6.30	3.30	0.42-3.33	0.42-3.33	0.42
5.90	6.28	3.90	0.50-3.00	0.50-3.00	0.50
3.00	7.00	7.20	0.25-1.25	0.25-3.25	0.50
8.00	4.00	5.60	0.50-4.00	0.50-2.00	0.50
8.00	5.60	4.00	0.50-4.00	0.50-2.50	0.50
8.00	3.20	8.00	0.50-4.00	0.50-1.50	0.50
8.00	8.00	3.20	0.50-4.00	0.50-4.00	0.50
8.30	8.00	5.00	0.42-4.17	0.42-4.17	0.42
9.20	7.50	5.80	0.50-5.00	0.50-4.00	0.50
7.50	7.50	7.50	0.50-5.00	0.50-5.00	0.50
4.40	9.50	11.00	0.37-2.20	0.37-4.77	0.36
10.00	10.00	10.00	0.50-5.00	0.50-5.00	0.50

The datasets for training and testing RFRs contain 1731 groups of perforated enclosures which are listed in Table I.

One perforated enclosure is selected to illustrate the details of its electric structural dimensions. Its enclosure dimensions are 5.00λ × 4.00λ × 3.20λ, and the initial size of the rectangular aperture on this enclosure is 0.25λ × 0.25λ, it is then extended to the maximum size of 4.25λ × 2.25λ with the step length of 0.25λ in *w/X* and *h/Y* direction, respectively. In addition, whatever the aperture size is, the aperture center remains located at the illuminated enclosure wall center.

For training the RFRs, 80% of the dataset, 1385 groups of perforated enclosure models, are randomly selected as the training set. And for the rest 20% of the dataset, 346 groups of perforated enclosure models, are selected as the testing set to cross-validate the performance of the established RFRs.

During the establishing process, RFR employs bagging technique [24] and random subspace [25] to construct a large set

of decision trees. Bagging means repeatedly selecting random samples with replacement of the training set and setting the selected samples as the training set for each decision tree. This means the training sets for each decision tree could be different. The selected samples are in the bag, about two-thirds of the total samples, and the remaining samples are called out-of-bag (OOB) for testing the performance of the corresponding decision tree. The Bagging process can ensure the independence of each decision tree. In the process of constructing the decision tree, random subspace means that each split node randomly extracts the feature subspace from the total feature space, which contains the structural dimensions of the perforated enclosure, as the candidate feature set of nodes, and selects the optimal feature to split. In this way, it not only ensures the nodes of each decision tree as well as the feature subspace between each tree node are different but also guarantees the independence and diversity of decision trees. The number of decision trees mainly affects the performance of the RFR.

The RFR establishing process mainly includes four steps.

Step 1: Use bagging to generate random training sample subsets for each decision tree.

Step 2: Generate random subspace. Feature subspaces are randomly extracted for node splitting and a single decision tree is constructed after validating by the OOB samples.

Step 3: Repeat step 1 and step 2 to construct all decision trees to form a forest.

Step 4: Output the predicted targets. The predicted values of all decision trees are averaged as the final predicted results.

The decision trees of the RFR algorithm adopt the classification and regression tree method. The generation of a decision tree is the process of constructing binary decision tree recursively, and the square error minimization criterion is used for the regression tree. Suppose X are the input variables as in (1) and x_j denotes the jth feature of X. Y contains variances which are the corresponding output variables. Each regression tree is generated as follows.

Obtain the training set for each regression tree by bagging technique. In each feature subspace, for the splitting variable j and the corresponding splitting point s, which equals to x_j, iterate the feature j to choose the pair (j, s) which minimizes the formula (2)

$$\min_{j,s}\left[\min_{c_1}\sum_{x_i\in R_1(j,s)}(y_i-c_1)^2+\min_{c_2}\sum_{x_i\in R_2(j,s)}(y_i-c_2)^2\right] \tag{2}$$

where $R_1(j,s)$ is the subregion with $x_i < s$, $R_2(j,s)$ is the subregion with $x_i \geq s$, c_1 is the mean value of y_i related to x_i in $R_1(j,s)$, and c_2 is the mean value of y_i related to x_i in $R_2(j,s)$. This process runs recursively on the nonleaf branches, until all data are processed and meet the termination criterion. The output of a regression tree is

$$f(x)=\sum_{m=1}^{M}c_m I(x\in R_m) \tag{3}$$

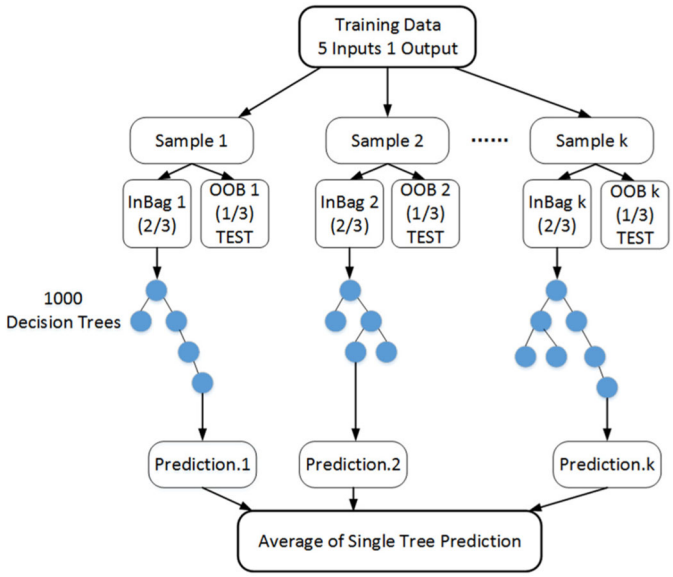

Fig. 3. Flowchart of RFR.

TABLE II
R^2 VALUES OF THE TRAINING SET AND TESTING SET FOR EACH RFR

RFRs for Variances	R^2	
	Training Set	Testing Set
σ_{Exr}^2	0.949	0.797
σ_{Eyr}^2	0.980	0.884
σ_{Ezr}^2	0.928	0.830
σ_{Exi}^2	0.968	0.877
σ_{Eyi}^2	0.980	0.870
σ_{Ezi}^2	0.966	0.890

where M is the total number of subregions, I is the input value in R_m, which is the mth subregion, and c_m is the mean value of the output variables in the mth subregion. Repeat this process, multitude regression trees will be generated to form the RFR.

The flowchart of RFR is shown in Fig. 3.

In this paper, six RFRs with 1000 decision trees are trained respectively. The performance of RFR is evaluated by the coefficient of determination R^2

$$R^2=1-\frac{\sum_{i=1}^{N}\left(Q_i-\hat{Q}_i\right)^2}{\sum_{i=1}^{N}\left(Q_i-\bar{Q}_i\right)^2} \tag{4}$$

where Q_i is the actual value, $\hat{Q}_i$ is the predicted value, $\bar{Q}_i$ is the mean value of the actual values, and N is the number of predicted targets. The R^2 values of the training set and testing set for each RFR are given in Table II.

The R^2 values are all close to 1 which indicates the high prediction accuracy and good generalization ability of the RFRs. The training time for each RFR is less than 60 s on the computer with the processor AMD RYZEN 7 1700 8 Core 3.0 GHz. Due to the electric dimensions in the training sets, the proposed RFR can be used to reconstruct the overall statistical characteristics of electric fields in perforated enclosures with the electric dimensions less than ten times the wavelength.

TABLE III
VARIANCES PREDICTED BY RFRS AND CALCULATED BY FULL WAVE SIMULATION OF THE REAL AND IMAGINARY PARTS OF THE RECTANGULAR ELECTRIC FIELD COMPONENTS IN THE EXAMPLE PERFORATED ENCLOSURE

Variances	RFR	Full Wave Simulation
$\sigma^2_{E_{xr}}$	8.09×10^{-5}	8.26×10^{-5}
$\sigma^2_{E_{xi}}$	9.09×10^{-5}	8.93×10^{-5}
$\sigma^2_{E_{yr}}$	0.5454	0.5455
$\sigma^2_{E_{yi}}$	0.0958	0.0927
$\sigma^2_{E_{zr}}$	0.2673	0.2673
$\sigma^2_{E_{zi}}$	0.0196	0.0196

IV. RECONSTRUCT STATISTICAL CHARACTERISTICS OF ELECTRIC FIELDS IN PERFORATED ENCLOSURES

In this section, with the assumption that E_{xr}, E_{xi}, E_{yr}, E_{yi}, E_{zr}, and E_{zi} in a perforated enclosure approximately obey normal distribution, the PDFs representing them are generated as normal distributions with the predicted variances and zero mean value. And then the generated PDFs are used to calculate the statistics of other electric fields by an analytical method and the MC method.

One perforated enclosure is selected from RFRs testing sets to illustrate the process of reconstructing the statistical characteristics of its internal electric fields. The physical dimensions of this enclosure are $A\_Enc = 295$ mm, $B\_Enc = 314$ mm, $C\_Enc = 195$ mm, $w\_Ape = 75$ mm, and $h\_Ape = 25$ mm. It is under the external plane wave illumination at 6 GHz, so its electric dimensions are $A\_Enc = 5.90\lambda$, $B\_Enc = 6.28\lambda$, $C\_Enc = 3.90\lambda$, $w\_Ape = 1.50\lambda$, and $h\_Ape = 0.50\lambda$, where λ is the wavelength of the incident plane wave. After inputting these five electric parameters into the six RFRs respectively, the variances of E_{xr}, E_{xi}, E_{yr}, E_{yi}, E_{zr}, and E_{zi} in this perforated enclosure can be immediately predicted. The predicted variances are listed in Table III and compared with the ones calculated by full wave simulation.

The good agreements between predicted and calculated variances prove the accuracy of the established RFRs. Then the predicted variances are substituted in (5), the PDF of the normal distribution, to approximately represent the PDFs of E_{xr}, E_{xi}, E_{yr}, E_{yi}, E_{zr}, and E_{zi}

$$f\left(x|\mu,\sigma^2\right) = \frac{1}{\sqrt{2\pi\sigma^2}} e^{-\frac{(x-\mu)^2}{2\sigma^2}} \tag{5}$$

where μ is the mean value and σ^2 is the variance.

The six normal distributions are compared with the corresponding PDFs calculated by full wave simulation as shown in Fig. 4.

In Fig. 4(a) and (b), the PDFs of E_{xr} and E_{xi} calculated by full wave simulation are sharper than the normal distributions generated with their predicted variances. It means the probability of E_{xr} and E_{xi} around zero is larger than the probability given by the normal distributions. However, the differences between the PDFs have less influence because comparing with E_{yr}, E_{yi}, E_{zr}, and E_{zi}, which are in the polarization and propagation directions of the incident plane wave, E_{xr} and E_{xi} have relatively small weights when calculating the overall statistical characteristics of

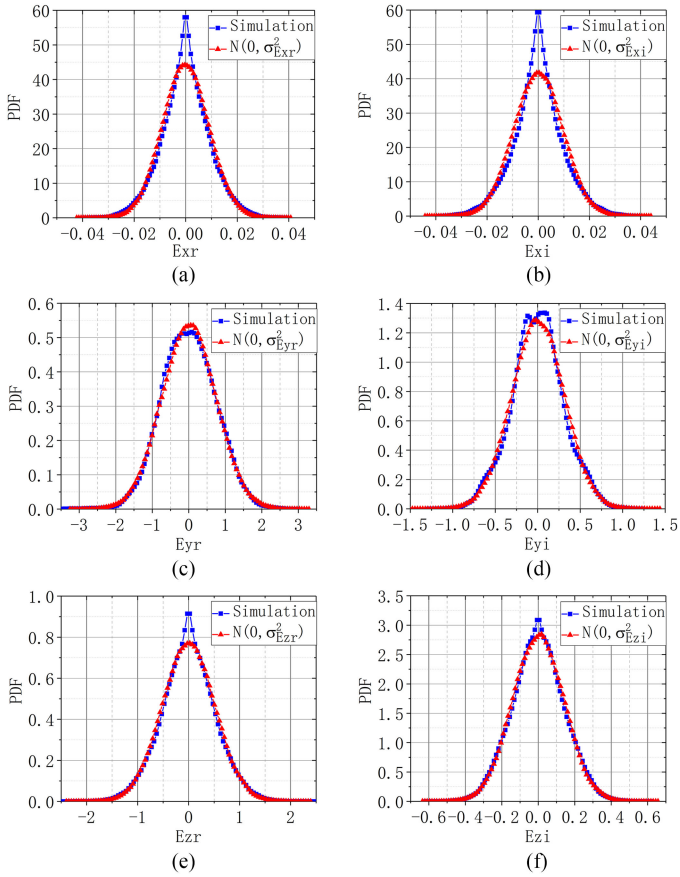

Fig. 4. PDFs calculated by full wave simulation and normal distributions generated with the variances predicted by RFRs. (a) E_{xr}. (b) E_{xi}. (c) E_{yr}. (d) E_{yi}. (e) E_{zr}. (f) E_{zi}.

the electric fields in this perforated enclosure. And the PDFs of E_{yr}, E_{yi}, E_{zr}, and E_{zi}, respectively, are in good agreements from the comparisons in Fig. 4, which suggests the normal distributions are suitable to approximately represent them.

After obtaining the PDF of E_{xr}, the mean values of other electric fields such as E^2_{xr}, the squared magnitude of rectangular electric field component such as $|E_x|^2$, and the squared magnitude of the total electric field $|\boldsymbol{E}|^2$, as well as the corresponding electric fields in y- and z-directions, can be directly calculated by analytical method. The complete statistical characteristics of the remaining electric fields can be calculated by MC method. The use of these two methods to reconstruct the statistical characteristics of electric fields in this perforated enclosure is discussed below.

A. Analytical Method to Calculate the Mean Values of the Electric Fields

In this part, the electric fields in x-direction are illustrated to calculate their mean values by analytical method [20]. Given a variable x to represent E_{xr} which is assumed to obey normal distribution, and the dependent variable y to represent E^2_{xr}, then $y = x^2$. Based on probability theory, the mean value of E^2_{xr} which denoted as $\langle E^2_{xr}\rangle$ can be expressed in term of the x^2 and

TABLE IV
MEAN VALUES AND STANDARD DEVIATIONS OF THE ELECTRIC FIELDS CALCULATED BY FULL WAVE SIMULATION, MONTE CARLO METHOD, AND ANALYTICAL METHOD IN THE EXAMPLE PERFORATED ENCLOSURE

	Mean Values			Standard Deviations	
	Simulation	MC	Analytical	Simulation	MC
$\|E_x\|$	0.0109	**0.0116**	×	0.0072	**0.0061**
$\|E_y\|$	0.6562	**0.6841**	×	0.4556	**0.4156**
$\|E_z\|$	0.4274	**0.4496**	×	0.3229	**0.2965**
$\|E\|$	0.8584	**0.8750**	×	0.4341	**0.4054**
$\|E_x\|^2$	1.7187×10^{-4}	$\mathbf{1.7162\times10^{-4}}$	$\mathbf{1.7180\times10^{-4}}$	2.2065×10^{-4}	$\mathbf{1.7210\times10^{-4}}$
$\|E_y\|^2$	0.6382	**0.6407**	**0.6412**	0.9070	**0.7835**
$\|E_z\|^2$	0.2869	**0.2872**	**0.2869**	0.4213	**0.3804**
$\|E\|^2$	0.9253	**0.9281**	**0.9282**	0.9734	**0.8748**

the PDF of x, as given in (6)

$$\langle y\rangle = \int_{-\infty}^{+\infty} x^2 \frac{1}{\sqrt{2\pi\sigma^2}} e^{-\frac{x^2}{2\sigma^2}} dx = \sigma^2 \tag{6}$$

where σ^2 is the variance of E_{xr}. Equation (6) indicates that with RFR, both $\sigma^2_{E_{xr}}$ and $\langle E^2_{xr}\rangle$ can be directly predicted. Therefore, the other mean values $\langle E^2_{xi}\rangle$, $\langle E^2_{yr}\rangle$, $\langle E^2_{yi}\rangle$, $\langle E^2_{zr}\rangle$, and $\langle E^2_{zi}\rangle$ can be directly obtained as they equal to the predicted variances of E_{xi}, E_{yr}, E_{yi}, E_{zr}, and E_{zi}. Furthermore, the mean values of $|E_x|^2$, $|E_y|^2$, $|E_z|^2$, and $|\boldsymbol{E}|^2$ can be calculated by using (7)

$$\langle |E_x|^2\rangle = \langle E^2_{xr}\rangle + \langle E^2_{xi}\rangle \tag{7a}$$

$$\langle |E_y|^2\rangle = \langle E^2_{yr}\rangle + \langle E^2_{yi}\rangle \tag{7b}$$

$$\langle |E_z|^2\rangle = \langle E^2_{zr}\rangle + \langle E^2_{zi}\rangle \tag{7c}$$

$$\langle |\boldsymbol{E}|^2\rangle = \langle |E_x|^2\rangle + \langle |E_y|^2\rangle + \langle |E_z|^2\rangle. \tag{7d}$$

The mean values of the squared electric fields calculated by (7) are given in Table IV to compare with the results calculated by the MC method and full wave simulation.

B. Monte Carlo Method to Calculate the Statistical Characteristics of the Electric Fields

In this part, the MC method is adopted to calculate the statistical characteristics of the electric fields which are not convenient to directly obtain by the analytical method. First, the predicted variances of E_{xr}, E_{xi}, E_{yr}, E_{yi}, E_{zr}, and E_{zi} are used to generate six sets of random numbers which obey normal distributions to represent them respectively. Each set has the same amount of random numbers as the sampling points in the full wave simulation. With the relationship, $|E_x| = \sqrt{E^2_{xr} + E^2_{xi}}$, the random numbers representing $|E_x|$ can be directly calculated, as well as $|E_y|$ and $|E_z|$. Following this, their complete statistical characteristics can be extracted. The cumulative distribution functions (CDFs) and the quantile-quantile (Q–Q) plots of $|E_x|$, $|E_y|$, $|E_z|$, and the magnitude of total electric field $|\boldsymbol{E}|$ are given in Fig. 5.

The Q–Q plots with the quantiles of the simulated results (on the horizontal axis) are plotted against the quantiles of the MC predicted results (on the vertical axis). Every 0.01-quantile from 0.01-quantile to 1.00-quantile is displayed. The solid line is a reference that represents a perfect match between the two datasets.

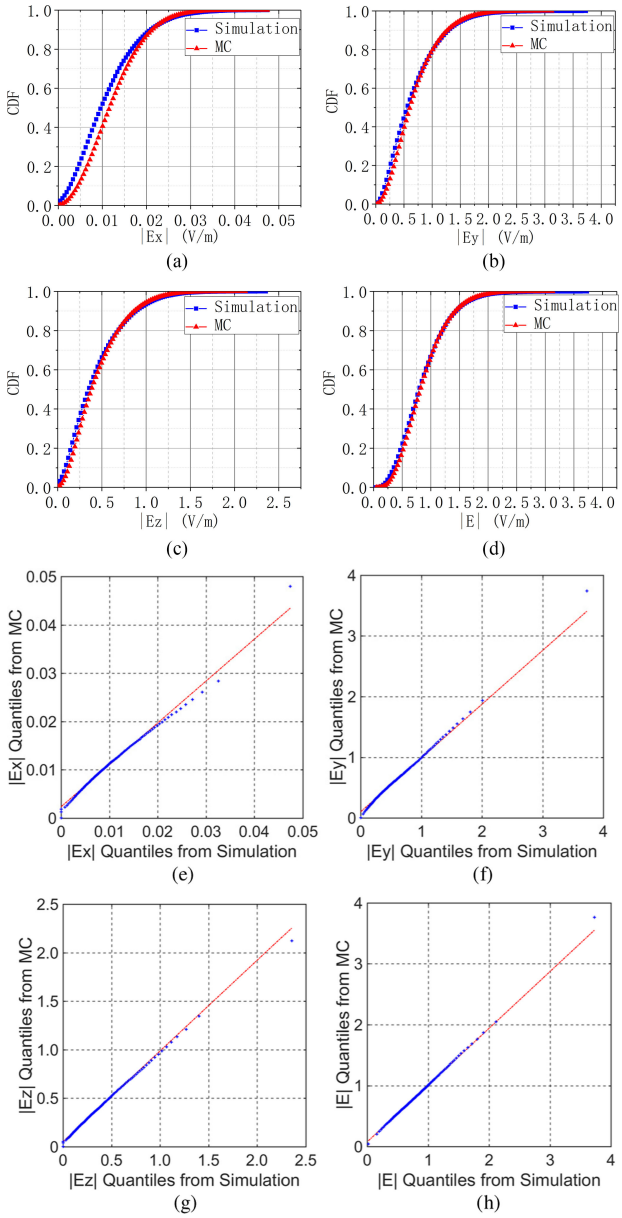

Fig. 5. CDFs and Q–Q plots of the electric field magnitudes calculated by MC method and full wave simulation. (a) $|E_x|$. (b) $|E_y|$. (c) $|E_z|$. (d) $|\boldsymbol{E}|$. (e) $|E_x|$. (f) $|E_y|$. (g) $|E_z|$. (h) $|\boldsymbol{E}|$.

The good agreements shown in Fig. 5 indicate the validity of generating random numbers by MC method to represent the electric fields in a perforated enclosure. The Q–Q plots indicate that the two datasets have very similar quantiles close to the reference line which further prove the agreement between the two datasets. The CDFs and the Q–Q plots of $|E_x|^2$, $|E_y|^2$, $|E_z|^2$, and $|\boldsymbol{E}|^2$ are also given in Fig. 6.

The CDFs and the Q–Q plots calculated by two methods are in good agreements, qualitative and quantitative information about the statistical characteristics of the electric fields can be intuitively observed. In Figs. 5 and 6, the outlier samples in the upper right corner present the deviations between the simulated results and the MC predicted ones at the 1.00-quantile. The other

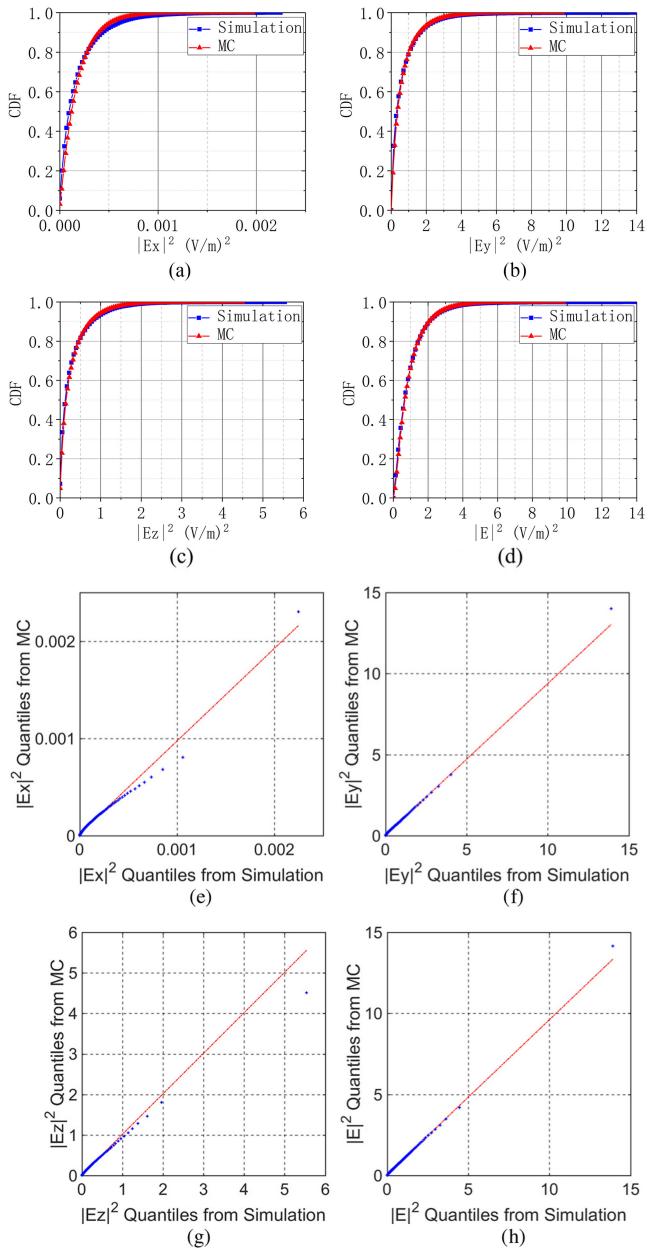

Fig. 6. CDFs and Q–Q plots of the squared electric field magnitudes calculated by MC method and full wave simulation. (a) $|E_x|^2$. (b) $|E_y|^2$. (c) $|E_z|^2$. (d) $|\boldsymbol{E}|^2$. (e) $|E_x|^2$. (f) $|E_y|^2$. (g) $|E_z|^2$. (h) $|\boldsymbol{E}|^2$.

two important statistics, mean values and standard deviations, of the electric fields calculated by MC method are given in Table IV to compare with the results obtained by the analytical method and full wave simulation.

The results given in Table IV indicate that the analytical method and the MC method can accurately calculate the mean values and standard deviations of the electric fields. Comparing with the rapid analytical method, the MC method can calculate the complete statistical characteristics of any electric fields in a perforated enclosure based on the generated random numbers.

Furthermore, the GSE of this perforated enclosure can be directly calculated as the ratio (in decibels) between the mean value of the total electric field magnitudes in absence of the enclosure $\langle|\boldsymbol{E}_{\rm o}|\rangle = 1.0$ V/m, and inside the enclosure $\langle|\boldsymbol{E}|\rangle = 0.875$ V/m as given in Table IV

$$\mathrm{GSE_{dB}} = 20\log\frac{\langle|E_0|\rangle}{\langle|E|\rangle} = 1.16\ \mathrm{dB}. \tag{8}$$

For this specific example, the lower GSE is resulted from the relatively large aperture and its longer side is perpendicular to the polarization direction of the incident plane wave. If we only consider the electric field strengths at several different positions in a perforated enclosure, the HFRS will be encountered and the overall characteristics of its internal EM environment will not be fully described. However, with the proposed method, these problems can be effectively overcome.

In addition, from the view of computational efforts, adopting the established RFRs to reconstruct the complete statistical characteristics of the electric fields in this perforated enclosure can be achieved in seconds. For undertaking the full wave simulation to analyze this model, it takes many hours on a computer with processor Intel (R) Core (TM) i5-4460 CPU 3.2 GHz.

V. Conclusion

In this paper, the good regularity of the electric field statistics in perforated enclosures is briefly reviewed first. It motivates us to establish a machine learning model RFR to build the relationship between the structural parameters of perforated enclosures and their internal electric field statistics. The electric dimensions of the enclosures and the apertures are selected as the input parameters of the RFRs, and the variances of real and imaginary parts of the three rectangular electric field components are selected as the predicted targets of the RFRs. Based on large amounts of training data, six RFRs are established respectively. With the predicted variances, the statistical characteristics of electric fields inside perforated enclosures can be quickly reconstructed by an analytical method and MC method. Some practical EMC issues such as GSE of perforated enclosures can be quickly evaluated by the predicted electric field mean values. Although the normal distribution can be simply constructed by the predicted variance, it does not achieve very accurate fitting for the real and imaginary parts of some rectangular electric field components. Their statistical characteristics fundamentally determine the statistical characteristics of the rectangular electric field components and the total electric field. Future works will focus on using generalized normal distributions to more accurately represent the PDF of the real and imaginary parts of the complex electric fields. It will further enable the PDFs of other electric fields and GSE to be obtained more accurately. Generalized normal distribution will introduce the shape and scale parameter as the additional predicted targets of the RFR. To include more general perforated enclosure structures, such as a single aperture and/or multiple apertures not centered on the illuminated wall of the unloaded or loaded enclosure, the positions of the apertures and the properties of the internal contents will be added as the input parameters to develop the generalization ability of the RFRs. Consequently, as the input parameter space increasing, some efficient sampling techniques will be considered.

REFERENCES

[1] A. Rabat, P. Bonnet, K. E. K. Drissi, and S. Girard, "Analytical models for electromagnetic coupling of an open metallic shield containing a loaded wire," *IEEE Trans. Electromagn. Compat.*, vol. 59, no. 5, pp. 1634–1637, Oct. 2017.

[2] W. P. Carpes, L. Pichon, and A. Razek, "Analysis of the coupling of an incident wave with a wire inside a cavity using an FEM in frequency and time domains," *IEEE Trans. Electromagn. Compat.*, vol. 44, no. 3, pp. 470–475, Aug. 2002.

[3] H. D. Brans, C. Schuster, and H. Singer, "Numerical electromagnetic field analysis for EMC problems," *IEEE Trans. Electromagn. Compat.*, vol. 49, no. 2, pp. 253–262, May 2007.

[4] Z. Yuan, Z. Xiang, Y. Liping, Z. Haijing, and H. Kama, "High frequency response sensitivity of electrically large enclosure with aperture and its statistical analysis method," in *Proc. Asia-Pacific Symp. Electromagn. Compat.*, Taipei, Taiwan, May 2015, pp. 185–188.

[5] R. Holland and R. H. S. John, *Statistical Electromagnetics*. Philadelphia, PA, USA: Taylor & Francis, 1999.

[6] G. Gradoni, J.-H. Yeh, B. Xiao, T. M. Antonsen, S. M. Anlage, and E. Ott, "Predicting the statistics of wave transport through chaotic cavities by the random coupling model: A review and recent progress," *Wave Motion*, vol. 51, no. 4, pp. 606–621, 2014.

[7] D. A. Hill, M. T. Ma, A. R. Ondrejka, B. F. Riddle, M. L. Crawford, and R. T. Johnk, "Aperture excitation of electrically large, lossy cavities," *IEEE Trans. Electromagn. Compat.*, vol. 36, no. 3, pp. 169–178, Aug. 1994.

[8] I. Junqua, J.-P. Parmantier, and F. Issac, "A network formulation of the power balance method for high frequency coupling," *Electromagnetics*, vol. 25, no. 7–8, pp. 603–622, 2005.

[9] I. D. Flintoft, S. L. Parker, S. J. Bale, A. C. Marvin, J. F. Dawson, and M. P. Robinson, "Measured average absorption cross-sections of printed circuit boards from 2 to 20 GHz," *IEEE Trans. Electromagn. Compat.*, vol. 58, no. 2, pp. 553–560, Apr. 2016.

[10] A. Gifuni, "A proposal to improve the standard on the shielding effectiveness measurements of materials and gaskets in a reverberation chamber," *IEEE Trans. Electromagn. Compat.*, vol. 59, no. 2, pp. 394–403, Apr. 2017.

[11] A. Gifuni *et al.*, "On the evaluation of the shielding effectiveness of an electrically large enclosure," *Adv. Electromag.*, vol. 1, no. 1, pp. 84–91, May 2012.

[12] C. L. Holloway *et al.*, "Use of reverberation chambers to determine the shielding effectiveness of physically small, electrically large enclosures and cavities," *IEEE Trans. Electromagn. Compat.*, vol. 50, no. 4, pp. 770–782, Nov. 2008.

[13] I. D. Flintoft *et al.*, "Representative contents design for shielding enclosure qualification form 2 to 20 GHz," *IEEE Trans. Electromagn. Compat.*, vol. 60, no. 1, pp. 173–181, Feb. 2018.

[14] I. D. Flintoft *et al.*, "Evaluation of the diffusion equation for modeling reverberant electromagnetic fields," *IEEE Trans. Electromagn. Compat.*, vol. 59, no. 3, pp. 760–769, Jun. 2017.

[15] J. Yan, J. Dawson, and A. Marvin, "Estimating reverberant electromagnetic fields in populated enclosures by using the diffusion model," in *Proc. 2018 IEEE Int. Symp. Electromagn. Compat., Signal Integrity Power Integrity*, Long Beach, CA, USA, Jul.–Aug. 2018, pp. 363–367.

[16] J. Yan, J. F. Dawson, A. C. Marvin, I. D. Flintoft, and M. P. Robinson, "3-D diffusion models for predicting reverberant electromagnetic power density in loaded enclosures," *IEEE Trans. Electromagn. Compat.*, to be published, doi: 10.1109/TEMC.2019.2916820.

[17] Y. Zhao, X. Zhao, L. Yan, H. Zhou, and K. Huang, "Statistical analysis of EM field distribution in the electrically large enclosure with different rectangle aperture," *J. Sichuan Univ.: Nature Sci. Ed.*, vol. 51, no. 4, pp. 738–744, Jul 2014.

[18] T. K. Ho, "Random decision forests," in *Proc. IEEE 3rd Int. Conf. Document Anal. Recognit.*, Aug. 1995, pp. 278–282.

[19] L. Breiman, "Random forests," *Mach. Learn.*, vol. 45, no. 1, pp. 5–32, 2001.

[20] A. Papoulis and S. Pillai, *Probability, Random Variables, and Stochastic Processes*, 3rd ed. New York, NY, USA: McGraw-Hill, 1991, pp. 142–143.

[21] Y. Li, X. Zhao, L. Yan, K. Huang, and H. Zhou, "Probabilistic-statistical model based on mode expansion of the EM field of a reverberation chamber and its Monte Carlo simulation," in *Proc. Asia-Pacific Symp. Electromagn. Compat.*, Shenzhen, China, May 18–21, 2016, pp. 779–781.

[22] S. Celozzi, "New figures of merit for the characterization of the performance of shielding enclosures," *IEEE Trans. Electromagn. Compat.*, vol. 46, no. 1, pp. 142–142, Feb. 2004.

[23] H. Li, H. Zhou, Y. Liu, X. Bao, and Z. Zhao, ''Massively parallel FDTD program JEMS-FDTD and its applications in platform coupling simulation," in *Proc. Int. Symp. Electromagn. Compat.*, Sep. 2014, pp. 229–233.

[24] L. Breiman, "Bagging predictors," *Mach. Learn.*, vol. 24, no. 2, pp. 123–140, 1996.

[25] T. K. Ho, "The random subspace method for constructing decision forests," *IEEE Trans. Pattern Anal. Mach. Intell.*, vol. 20, no. 8, pp. 832–844, Aug. 1998.

Yuan Zhao received the M.S. degree in radio physics from Sichuan University, Chengdu, China, in 2014. He is currently working towards the Ph.D. degree in radio physics at Sichuan University. From October 2017 to October 2018 he was a joint Ph.D. Student with the George Green Institute for Electromagnetics Research at the University of Nottingham, Nottingham, U.K.

His research interests include statistical electromagnetics, electromagnetic environment effects, electromagnetic compatibility modeling, and computational electromagnetic.

Xiang Zhao received the M.S. degree in radio physics and the Ph.D. degree in biomedical engineering from the Sichuan University, Chengdu, China, in 1997 and 2005, respectively.

In 1997, she joined the Department of Electronics Engineering at Sichuan University. Since 2012, she has been a Professor with the College of Electronics and Information Engineering, Sichuan University, Chengdu, China. She has authored or co-authored over 90 papers in the peer-reviewed journals and conferences, and led a number of grant projects. Her research interests include statistical electromagnetics, electromagnetic compatibility modeling, and electromagnetic environment effects evaluation.

Liping Yan (M'08–SM'15) received the M.S. degree in radio physics and the Ph.D. degree in biomedical engineering from Sichuan University, Chengdu, China, in 1996 and 2003, respectively.

In 1996, she joined the Department of Electronics Engineering at Sichuan University. From March 2008 to March 2009, she was a Visiting Scholar with the Department of Electrical Engineering and Computer Science, University of Wisconsin, Milwaukee, USA. Since July 2009, she has been working as a Professor with the College of Electronics and Information Engineering, Sichuan University, Chengdu, China.

She has authored/co-authored one book, more than 100 papers published in peer-reviewed journals and international conferences and led a number of industrial/grant projects. Her research interests include electromagnetic environment effects, electromagnetic compatibility modeling, computational electromagnetics, design of applicators/probes for biomedical applications, and compact antennas.

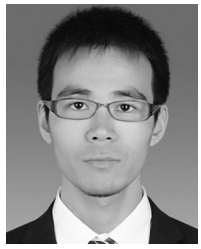

Zhengyang Liu received the B.S degree in telecommunication engineering from Sichuan University, Chengdu, China, in 2016, and he is currently working toward the M.S degree from Sichuan University, Chengdu, China.

His current research interests include the performance shielding effectiveness of loaded cavity, the application of neural network in electromagnetic compatibility.

Qiang Liu received the B.S. degree in electronic engineering from the University of Electronics Science and Technology in 1991, and the M.S. degree in electronic engineering from Sichuan University in 2010.

He is currently an Associate Professor with the Institute of Applied Physics and Computational Mathematics, Beijing, China. His current interests include electromagnetic environment effects, computational electromagnetics, statistical electromagnetics, and microwave engineering.

Changjun Liu (M'07–SM'09) received the B.S. degree in applied physics from Hebei University, Baoding, China, in 1994, and the M.S. degree in radio physics and the Ph.D. degree in biomedical engineering from Sichuan University, Chengdu, China, in 1997 and 2000, respectively.

From 2000 to 2001, he was a Postdoctoral Researcher with Seoul National University, Seoul, South Korea. From 2006 to 2007, he was a Visiting Scholar with Ulm University, Ulm, Germany. Since1997, he has been with the Department of Radio-Electronics, Sichuan University, where he has been a Professor since 2004. He has authored one book, one chapter in a book, and more than 100 articles. He holds more than ten patents. His current research interests include microwave power combining of large-power vacuum components, microwave wireless power transmission, and microwave power industrial applications.

Dr. Liu was a recipient of several honors, such as the Outstanding Reviewer of the IEEE TRANSACTIONS ON MICROWAVE THEORY AND TECHNIQUES from 2006 to 2010, support from the Ministry of Education (MOE) under the Program for New Century Excellent Talents in University, China, from 2012 to 2014, the Sichuan Province Outstanding Youth Fund from 2009 to 2012, and named by Sichuan Province as an Expert with Outstanding Contribution from 2008 to 2013. He serves on the editorial board of the Chinese Journal of Applied Science.

Haijing Zhou received the B.S., M.S., and Ph.D. degrees in microwave engineering from the University of Electronics Science and Technology of China, Chengdu, China, in 1991, 1994, and 1997, respectively.

He is currently a Professor with the Institute of Applied Physics and Computational Mathematics, Beijing. His current interests include transient electromagnetics, computational electromagnetics, microwave technology, antenna technology, and wave propagation.

Kama Huang (M'01–SM'04) received the M.S. and Ph.D. degrees in microwave theory and technology from the University of Electronic Science and Technology, Chengdu, China, in 1988 and 1991, respectively.

Since 1994, he has been a Professor with the School of Electronics and Information Engineering, Sichuan University, Chengdu, where he has been the Director of the School of Electronics and Information Engineering since 1997. In 1996, 1997, 1999, and 2001, he was a Visiting Scientist with the Scientific Research Center Vidhuk, Kiev, Ukraine, with the Institute of Biophysics CNR, Pisa, Italy, with the Technical University Vienna, Vienna, Austria, and also with Clemson University, Clemson, SC, USA, respectively.